Am J Transl Res 2022;14(6):4321-4336
www.ajtr.org /ISSN:1943-8141/AJTR0142061

Original Article

Total glucosides of paeony inhibits liver fibrosis and inflammatory response associated with cirrhosis via the FLI1/NLRP3 axis

Jie Zhang[1], Yiwei Fu[1], Bin Yang[1], Xiaoxing Xiang[2]

[1]*Department of Gastroenterology, Taizhou People's Hospital Affiliated to Medical College of Yangzhou University, Taizhou 225300, Jiangsu, P. R. China;* [2]*Yangzhou University Medical College, Yangzhou 225009, Jiangsu, P. R. China*

Received January 27, 2022; Accepted April 1, 2022; Epub June 15, 2022; Published June 30, 2022

Abstract: Background: Total glucosides of paeony (TGP) has a myriad of hepatoprotective activities. However, its role in cirrhosis, a major risk factor for hepatocellular carcinoma, remains largely unexplored. Here, we determined the impact of TGP on liver fibrosis and inflammation in mice modeled by carbon tetrachloride with an aim to explore a possible molecular mechanism. Methods: Liver fibrosis and inflammation in mice were evaluated using ELISA, hematoxylin-eosin, Masson's trichrome, immunohistochemical staining and TUNEL methods. The impact of TGP on gene expression in the liver tissues of the mice was investigated using microarray analysis, showing the most significant increase in expression of friend leukemia integration 1 transcription factor (FLI1). After loss-of-functions assays of FLI1, the downstream gene of FLI1 was searched by bioinformatics analysis and verified. Results: TGP reduced liver tissue damage, inhibited apoptosis, and alleviated liver fibrosis and inflammation in cirrhotic mice. FLI1 was downregulated in the liver of cirrhotic mice and lipopolysaccharide-treated hepatocytes, and TGP promoted the expression of FLI1. FLI1 depletion inhibited the effects of TGP on alleviating liver fibrosis and inflammatory responses in mice. FLI1 repressed Nod-like receptor protein 3 (NLRP3) transcription by binding to its promoter. Further silencing of NLRP3 in the presence of shFLI1 alleviated histopathological changes, inhibited apoptosis, and attenuated liver fibrosis and inflammatory responses in the liver of cirrhotic mice. Conclusions: TGP promotes the expression of FLI1, which in turn inhibits NLRP3 expression, thereby reducing cirrhosis-induced liver fibrosis and inflammatory response in mice.

Keywords: Total glucosides of paeony, cirrhosis, FLI1, NLRP3, liver fibrosis

Introduction

Liver cirrhosis is a main driver of morbidity and mortality in developed countries with a one-year mortality rate ranging from 1% to 57% depending on the stage [1]. Cirrhosis develops after chronic inflammation that contributes to replacement of the healthy liver parenchyma with fibrotic tissues and regenerative nodules, leading to portal hypertension [2]. The loss of functional hepatocytes leads to the weakening of liver function, such as the ability to metabolize bilirubin and synthesize proteins [3]. The mechanisms of combating liver fibrosis can be summarized as follows: elimination of injurious factors causing chronic hepatic damage, removal of myofibroblasts, impairment of inflammatory response and activation of anti-inflammatory pathways [4]. Nevertheless, the reversal is often too slow or too sporadic to avoid life-threatening complications, especially in advanced fibrosis [5]. As a consequence, there is an unmet medical need for anti-fibrotic therapies to reverse cirrhosis progression.

Paeoniae Radix Alba, the root of *Paeonia lactiflora Pall.*, has been applied as a traditional medicine for autoimmune diseases related to inflammatory response, and total glucosides of paeony (TGP), the principal active component of Paeoniae Radix Alba, has been verified to show anti-inflammatory and analgesic effects [6]. The alleviating effects of TGP have been well-described in ankylosing spondylitis [7],

arthritis [8], as well as Sjogren's syndrome [9]. Single-dose of TGP capsule has been recently found to effectively reduce serum total bile acid in rats with hepatic injury [10]. Also, TGP decreased apoptosis of hepatocytes through the mitochondrial apoptotic pathway in autoimmune hepatitis [11]. In addition, Paeoniflorin (PAE, C23H28O11), the main bioactive components of TGP, exerts protective effect on hepatic fibrosis in rats subjected to radiation [12]. However, the efficacy of TGP on cirrhosis-associated fibrosis and inflammatory responses is less understood. In the present study, we injected carbon tetrachloride (CCl_4) to induce cirrhotic mice [13], followed by microarray analysis of differentially expressed genes between cirrhotic mice and normal mice. It was thus revealed that friend leukemia integration 1 transcription factor (FLI1) was a possible candidate target of TGP in cirrhosis. FLI1, a member of the Ets family, partakes in the development, proliferation, activation and migration of immune cells [14]. Transcription factor FLI1 has been shown to hamper collagen synthesis in cultured dermal fibroblasts [15]. Nevertheless, no conclusive evidence has been found regarding the effects of FLI1 on cirrhosis. We therefore hypothesized that one of the possible mechanisms for the anti-fibrotic, anti-inflammatory and anti-apoptotic properties of TGP in cirrhosis is mediated through the upregulation of FLI1 expression.

Materials and methods

Mice

Sixty-six male C57BL/6 mice (6 weeks old) were acquired from Shanghai Lab Animal Research Center (Shanghai, China). All mice were maintained in a humidity- (55-65%) and temperature-controlled (23 ± 2°C) environment under *ad libitum* supply of food and water and a 12/12 h day-night cycle. The animal study was ratified by the Ethics Committee of Medical College of Yangzhou University (Approval number: 2021-067-02) and performed following *The Guide for the Care and Use of Laboratory Animals* published by the US NIH (publication No. 85-23, revised 1996).

CCl_4-induced cirrhosis and treatment

After one week of adaptive feeding, cirrhotic mice (n = 42) were developed by subcutaneous injection of CCl_4 diluted in olive oil (1:1, v/v) two times a week (2 mL/kg) for 6 weeks. The remaining 24 mice were simultaneously injected with equal amount of olive oil and further classified into four groups: the control group (n = 6, no additional treatment), TGP group (n = 6, intragastrical administration of TGP), AAV-NC group (n = 6, tail vein injection of adenovirus AAV-NC), and AAV-shFLI1 group (n = 6, tail vein injection of adenovirus AAV-shFLI1).

The cirrhotic mice were randomly allocated into seven groups: the CCl_4 (n = 6, cirrhotic mouse model), CCl_4 + TGP (n = 6, cirrhotic mice subjected to intragastrical administration of TGP), AAV-NC (n = 6, cirrhotic mice subjected to intragastrical administration of TGP and tail vein injection of adenovirus AAV-NC), AAV-shFLI1 (n = 6, cirrhotic mice subjected to intragastrical administration of TGP and tail vein injection of adenovirus AAV-shFLI1), AAV-NC + AAV-shFLI1 (n = 6, cirrhotic mice subjected to intragastrical administration of TGP and tail vein injection of adenoviruses AAV-shFLI1 and AAV-NC), AAV-NC + AAV-shNLRP3 (n = 6, cirrhotic mice subjected to intragastrical administration of TGP and tail vein injection of adenoviruses AAV-shNLRP3 and AAV-NC) and AAV-shFLI1 + AAV-sh-NLRP3 (n = 6, cirrhotic mice subjected to intragastrical administration of TGP and tail vein injection of adenoviruses AAV-shFLI1 and AAV sh-NLRP3).

Intragastrical administration of TGP (Ningbo Liwah Pharmaceutical Co., Ltd., Ningbo, Zhejiang, China) at 200 mg/kg (suspended in 0.9% sterile NaCl) once daily for 3 weeks was started at the 4th week of olive oil (containing CCl_4 or not) injection.

AAV-shFLI1, AAV-sh-NLRP3 and empty adenoviral vector AAV-NC were provided by GenePharma (Shanghai, China). Mice requiring adenovirus treatment were injected with 200 μL adenovirus (1 × 10^9 TU/mL) in the tail vein twice a week for 2 weeks, starting at the 5th week of CCl_4 injection. All mice were euthanized after 6 weeks, and the livers were removed for following assays.

Enzyme-linked immunosorbent assay (ELISA)

Mouse serum was centrifuged at 1500 g for 10 min at 4°C. The levels of liver injury markers ALT (ab282882) and AST (ab263882) in mouse serum were evaluated using ELISA kits (Abcam,

Cambridge, UK). The concentrations of TNF-α (MTA00B), IL-1β (MLB00C) and IL-6 (M6000B) in the serum of mice were measured by ELISA kits (R&D Systems, Minneapolis, MN, USA).

HE staining

Pathological changes in the liver of mice were detected by HE staining as per the instructions of the HE staining kit (Beyotime, Shanghai, China). Mouse liver tissues were fixed with 4% paraformaldehyde, paraffin-embedded, and sliced into 4-μm-thick sections. The above sections were dewaxed with xylene, hydrated with ethanol at gradient concentrations, stained with hematoxylin for 5 min at room temperature, treated with 5% acetic acid for 1 min, and stained with eosin for 1 min. Pathological changes in the liver sections were viewed under a microscope (Olympus Optical Co., Ltd., Tokyo, Japan) after routine dehydration, clearance and sealing.

Masson's trichrome staining

Fibrosis in mouse liver tissues was detected using the Masson's kit (Servicebio, Wuhan, Hubei, China). Mouse liver tissues were fixed in 4% paraformaldehyde overnight and paraffin-embedded. The 4-μm sections were stained with Masson's trichrome and examined with Image Pro Plus v7.0 software for fibrosis area analysis. In each section, five random views were captured under a light microscope. The percentage of fibrotic area was measured by comparing the collagen staining area with the total area.

Immunohistochemistry

Paraffin-embedded sections of mouse liver tissues were dewaxed with xylene and rehydrated with ethanol at gradient concentrations. Rehydrated tissue sections were incubated in 3% H_2O_2 for 20 min at room temperature and sealed with 100 μL 5% BSA at 37°C for 30 min. The sections were probed with primary antibody against α-SMA (1:1000, ab124964, Abcam) overnight at 4°C and with HRP-labeled secondary goat anti-rabbit antibody against IgG H&L (1:5000, ab205718, Abcam) for 1 h at room temperature. Finally, the sections were treated with DAB (Roche Diagnostics, Indianapolis, IN, USA) and counter-stained with hematoxylin for 30 s before dehydration and fixation. Images were viewed under a confocal microscope LSM710 (Zeiss, Oberkochen, Germany) and quantitatively analyzed by Image Pro Plus v7.0.

TUNEL assay

Hepatocyte apoptosis was evaluated using the TUNEL Assay Apoptosis Detection Kit (Solarbio, Beijing, China). Liver tissues were sliced into 4-μm paraffin-embedded sections, dewaxed, hydrated, and treated with proteinase K solution for 15 min at room temperature. The sections were cultured with 500 μL TUNEL reaction mixture at 37°C for 1 h and reacted with 100 μL DAB substrate for 10 min. After hematoxylin counter-staining, the sections were sealed with neutral gum. Apoptotic cell nuclei (in yellow-brown or dark brown) were observed under an optical microscope (Eclipse TE2000-U, Nikon Instruments Inc., Melville, NY, USA), and the apoptotic rate was calculated as number of apoptotic nuclei/total nuclei.

Microarray analysis

Transcriptome differences in mouse liver due to TGP treatment was analyzed using a mouse GE 4 × 44 K v2 microarray kit (Agilent Technologies, Santa Clara, CA, USA). Total RNA was isolated using a RNeasy mini kit (Qiagen, Valencia, CA, USA), followed by DNase treatment (RNase-Free DNase Set; Qiagen). The total RNA was reversely transcribed into cDNA. After the examination of RNA quality using an Agilent 2100 Bioanalyzer, RNA was labeled using a Low Input Quick Amp Labeling Kit (Agilent) and hybridized using the mouse gene expression microarrays for 17 h at 65°C. Sections were scanned on an Agilent SureScan Microarray Scanner (G2600D) and analyzed using the Feature Extraction Software 11.5.1.1 (Agilent).

RT-qPCR

Total RNA was isolated from hepatocytes and liver tissue using TRIzol (Invitrogen, Carlsbad, CA, USA). RNA concentration was measured using a NanoDrop 8000 spectrophotometer (Thermo Fisher Scientific Inc., Waltham, MA, USA). RNA was reversely transcribed to cDNA using the PrimeScript™ RT reagent Kit with gDNA Eraser (RR047A, Takara Biotechnology Ltd., Dalian, Liaoning, China). RT-qPCR was car-

Table 1. Primers used in RT-qPCR

Name of primer	Sequences (5'-3')
FLI1-F	CCATACAGACCAGTCCTCACGA
FLI1-R	CATGGTCTGTGATCCTCCAAGG
NLRP3-F	TCACAACTCGCCCAAGGAGGAA
NLRP3-R	AAGAGACCACGGCAGAAGCTAG
GAPDH-F	CATCACTGCCACCCAGAAGACTG
GAPDH-R	ATGCCAGTGAGCTTCCCGTTCAG

Note: FLI1, friend leukemia integration 1 transcription factor; NLRP3, nod-like receptor protein 3; GAPDH, glyceraldehyde-3-phosphate dehydrogenase; F, forward; R, reverse.

ried out using the TB Green® Premix Ex Taq™ (Takara) as per the manufacturer's instructions and performed on the CFX96 Real-Time PCR Detection System (Bio-Rad Laboratories, Hercules, CA, USA). Data analysis was conducted using the $2^{-\Delta\Delta CT}$ method and normalized to GAPDH. Primer sequences are provided in **Table 1**.

Western blot

We used radio immunoprecipitation assay lysis buffer (Solarbio) to obtain total protein from hepatocytes and mouse liver tissue. The protein concentrations were assessed using the BCA assay protein assay kit (Solarbio). Proteins (20 μg) were electrophoresed using 10% SDA-polyacrylamide gel and transferred onto PVDF membranes (Millipore Corp., Billerica, MA, USA). Membranes were sealed with 5% skim milk on a shaker for one hour at room temperature and probed with primary antibodies against FLI1 (1:1000, ab133485, Abcam), NLRP3 (1:1000, ab263899, Abcam), and GAPDH (1:10000, ab181602, Abcam) overnight at 4°C. The next day, the membranes were re-probed with secondary antibody goat anti-rabbit IgG H&L (HRP) (1:10,000, ab2057-18, Abcam) for 120 min at room temperature. Immunoreactive bands were measured using an ECL substrate kit (Abcam). Band intensities were quantified and analyzed by ImageJ (NIH, Bethesda, MD, USA).

Cell transfection

A mouse normal hepatocyte line NCTC 1469 (CCL-9.1) was purchased from ATCC (Manassas, VA, USA). The cells were cultured in DMEM containing 10% FBS, 100 U/mL penicillin, and 100 μg/mL streptomycin (Thermo Fisher Scientific, MA, USA) at 37°C and 5% CO_2.

The overexpressed DNA plasmid oe-FLI1 and the control were purchased from GenePharma. After induction of well-grown hepatocytes by lipopolysaccharide (LPS), oe-NC or oe-FLI1 was delivered into the induced cells using the lipfectamine 2000 transfection kit (Thermo Fisher Scientific).

Dual-luciferase assay

The potential binding site of FLI1 on the NLRP3 promoter sequence was downloaded from hTFtarget (http://bioinfo.life.hust.edu.cn/hTFtarget/#!/), and NLRP3 promoters containing the binding site (WT) or mutated binding site (MT) were inserted into the pPro-RB-Report vector (RiboBio) to generate a promoter luciferase reporter vector. The above vectors were co-transfected with overexpression of (oe)-NC or oe-FLI1 into NCTC 1469 cells using Lipofectamine 2000, respectively. After 2 d, luciferase assays were carried out using a dual-luciferase reporter gene assay system (Promega, Madison, WI, USA). The firefly luciferase activity was normalized to the Renilla luciferase activity.

ChIP

The Magna ChIP™ A/G ChIP Kit (Merck Millipore, Burlington, MA, USA) was used following the manufacturer's instructions. The cells were fixed using 4% paraformaldehyde, and the supernatant was harvested after a 5-min 13,000-rpm centrifugation at 4°C after sonication, and incubated overnight at 4°C with rabbit antibodies against FLI1 (1:50, #35980, CST, Beverly, MA, USA) or IgG (1:50, ab1727-30, Abcam), respectively. DNA fragments were purified by phenol/chloroform extraction and analyzed by qPCR.

Statistics

SPSS 22.0 software (IBM Corp., Armonk, NY, USA) was applied for statistical processing. Unpaired *t*-test was utilized to compare the data between two groups, and one-way ANOVA was used to compare data among multiple groups and followed by Tukey-test. $P < 0.05$ was accepted as statistically significant. All

numerical data were repeated at least 3 times and expressed as mean ± SD.

Results

TGP attenuates liver fibrosis and inflammatory response in mice

We established a mouse model of cirrhosis by CCl_4 treatment. As for control, mice were treated with olive oil. The expressions of ALT and AST, markers of liver injury in mouse serum, were detected by ELISA kits and found to be significantly increased in the CCl_4 group. After treatment of TGP, the expressions of ALT and AST in the serum of mice treated with CCl_4 were significantly reduced. TGP did not remarkably alter the expression of either in the serum of normal mice (**Figure 1A**). Subsequently, the liver tissue damage in mice was evaluated by HE staining. The control group had a clear structure of liver lobules, normal structure of the central vein and confluence area; hepatic cell cords arranged radially from the central vein to the surrounding area with irregular hepatic sinusoids, which was not significantly altered by TGP. By contrast, the mice in the CCl_4 group showed typical cirrhotic changes with extensive fibrous hyperplasia of liver stroma, more pseudobullets and diffuse inflammatory cell infiltration of interstitial tissue, which were significantly suppressed in the TGP group (**Figure 1B**). Masson's staining found that the liver tissue structure of control mice was normal and fibrous deposition was rarely seen, while the liver fibrous tissue of CCl_4-treated mice proliferated significantly and formed wider fibrous spacing. However, the collagen area of liver tissues in mice of the CCl_4 + TGP group was significantly reduced, and fibrosis was significantly suppressed (**Figure 1C**).

We then measured the expression of the fibrosis marker α-SMA by immunohistochemistry. Relative to the control group, the expression of α-SMA in the liver tissues of mice in the TGP group did not change significantly. The expression of α-SMA was much higher in the CCl_4 group, which was decreased by TGP treatment (**Figure 1D**). The results of TUNEL staining demonstrated that there were a small number of apoptotic hepatocytes in the liver tissues of control mice, and TGP showed no significant impact on apoptosis in the control mice. The pro-apoptotic effects of CCl_4 on hepatocytes was considerably inhibited after TGP treatment (**Figure 1E**). Finally, we tested the levels of TNF-α, IL-1β and IL-6 in the serum of mice. It was revealed that the release of TNF-α, IL-1β and IL-6 in the serum of mice was stimulated by CCl_4 injections, whereas TGP alleviated the inflammatory response in the serum of cirrhotic mice (**Figure 1F**). Therefore, TGP treatment alone did not produce significant toxic effects on normal mouse liver, but reduced liver tissue damage, inhibited apoptosis and attenuated liver fibrosis and inflammatory response in cirrhotic mice.

TGP partly reverses the downregulation of transcription factor FLI1 by CCl_4

Differences in gene expression profiles in the liver tissues of cirrhotic mouse resulting from TGP treatment were analyzed by microarray (**Figure 2A**). We found the most significant difference in FLI1 expression in mouse liver tissues with or without TGP treatment. We then evaluated the expression of FLI1 in mice using RT-qPCR and Western blot. FLI1 was considerably diminished in CCl_4-administrated mice, while FLI1 expression in the liver was partially increased after TGP treatment (**Figure 2B**, **2C**). We then downregulated the FLI1 expression in TGP-treated cirrhotic mice through tail vein injection of AAV-shFLI1 or AAV-NC. The result of RT-qPCR and Western blot results revealed that AAV-NC did not significantly affect FLI1 expression in the liver of TGP-treated cirrhotic mice, while AAV-shFLI1 significantly inhibited FLI1 expression in mouse liver tissues (**Figure 2D**, **2E**).

FLI1 inhibits the effects of TGP on alleviating liver fibrosis and inflammatory response in mice

The levels of ALT and AST were considerably augmented in mouse serum after inhibition of FLI1 by ELISA analysis (**Figure 3A**). The results of HE staining exhibited that mice in the AAV-shFLI1 group had increased liver pathology, enhanced pseudobullets and augmented inflammatory cell infiltration (**Figure 3B**). By Masson's staining, we observed that inhibition of FLI1 aggravated liver fibrosis in mice with a significant promotion in the collagen area of liver tissues (**Figure 3C**). Similar results were obtained by immunohistochemical analysis of the fibrosis marker α-SMA, and inhibition of FLI1 increased the expression of α-SMA (**Figure 3D**).

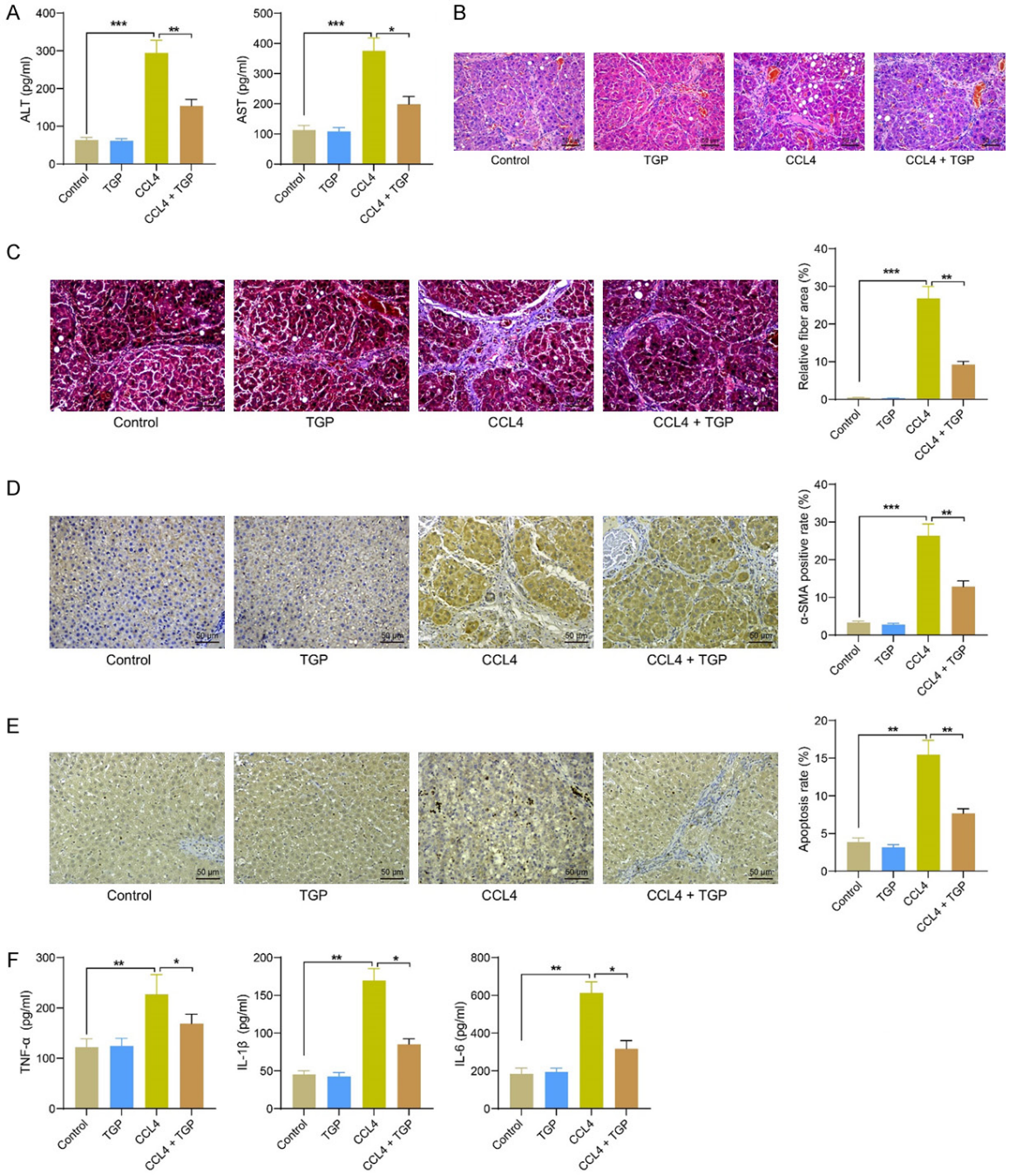

Figure 1. TGP attenuates cirrhosis-induced liver fibrosis and inflammation in mice. A. Detection of ALT and AST levels in serum of mice with cirrhosis by ELISA. B. The extent of liver tissue damage in cirrhotic mice assessed using HE staining. C. Fibrosis in the liver of cirrhotic mice measured using Masson's staining. D. Immunohistochemical analysis of α-SMA positivity in liver tissues of cirrhotic mice. E. Apoptosis in mice with liver cirrhosis measured using TUNEL assay. F. The determination of TNF-α, IL-1β and IL-6 in the serum of mice with cirrhosis examined using ELISA assay. Data are displayed as the mean ± SD (n = 6) and compared by one-way ANOVA. *P < 0.05, **P < 0.01, ***P < 0.001. TGP, total glucosides of paeony; ALT, alanine aminotransferase; AST, aspartate aminotransferase; ELISA, enzyme-linked immunosorbent assay; HE, hematoxylin-eosin; α-SMA, alpha skeletal muscle actin; TUNEL, terminal deoxynucleotidyl transferase (TdT)-mediated 2'-Deoxyuridine 5'-Triphosphate (dUTP) nick end labeling; TNF-α, tumor necrosis factor alpha; IL, interleukin.

TUNEL results showed that the apoptosis was significantly enhanced in the AAV-shFLI1-administrated mice (**Figure 3E**). Finally, ELISA analysis revealed a significant elevation in the

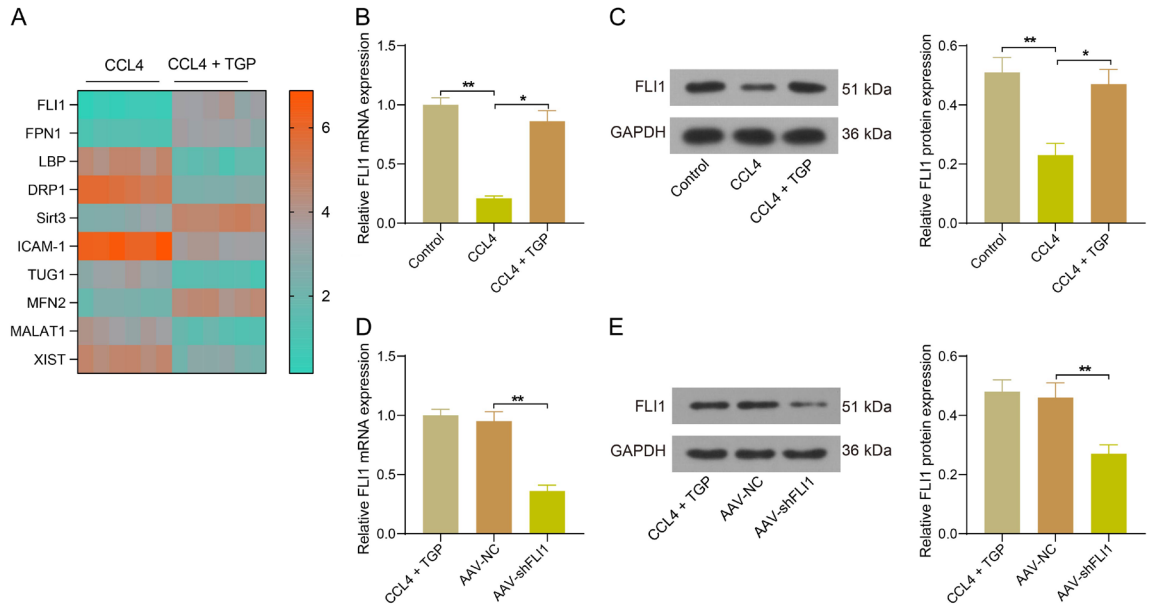

Figure 2. TGP can promote the expression of transcription factor FLI1. (A) Microarray analysis of differential gene expression profiles in the liver of mice treated with CCl_4 or CCl_4 + TGP. (B, C) Detection of FLI1 expression in liver tissues of mice by RT-qPCR (B) and Western blot (original, full-length gel and blot images can be found in the Supplementary Figure 1) (C). (D, E) Detection of FLI1 mRNA and protein expression after tail vein injection of AAV-shFLI1 or AAV-NC in CCl_4 + TGP-treated mice by RT-qPCR (D) and Western blot (original, full-length gel and blot images can be found in the Supplementary Figure 1) (E). Data are displayed as the mean ± SD (n = 6) and compared by one-way ANOVA. *P < 0.05, **P < 0.01. TGP, total glucosides of paeony; FLI1, friend leukemia integration 1 transcription factor; CCl_4, carbon tetrachloride; AAV, adeno-associated virus; NC, negative control.

serum levels of TNF-α, IL-1β and IL-6 in the AAV-shFLI1 group (**Figure 3F**). These data suggest that suppression of FLI1 exacerbates liver tissue damage, promotes apoptosis, increases liver fibrosis and inflammatory responses, and inhibits the protective effects of TGP in cirrhotic mice.

In addition, we treated normal mice with AAV-shFLI1 or AAV-NC. It was detected by Western blot that AAV-NC did not remarkably alter the expression of FLI1 in the normal mice, while AAV-shFLI1 successfully repressed the expression of FLI1 in the liver tissues (**Figure 3G**). We observed that inhibition of FLI1 induced mild inflammatory infiltration (**Figure 3H**) and collagen deposition (**Figure 3I**) in normal mouse liver tissues by HE staining and Masson's staining, respectively. Moreover, AAV-shFLI1 stimulated the progression of fibrosis in normal mouse liver tissues by immunohistochemical staining of α-SMA (**Figure 3J**). Therefore, FLI1 plays a role in maintaining the normal morphology of liver tissues and inhibiting the progression of fibrosis in the liver.

FLI1 represses NLRP3 transcription

To reveal the mechanism of action of FLI1 in liver fibrosis and inflammatory response, we downloaded potential downstream factors regulated by FLI1 from hTFtarget and selected the top one hundred targets for pathway enrichment analysis. We found that the highest enrichment was in the GO:0002366 pathway (**Figure 4A**). The proteins enriched in this pathway were chosen for their functional analysis in String (https://cn.string-db.org/), and we observed NLRP3 as the main downstream functional executor of these proteins (**Figure 4B**). Through the ChIP-seq database Cistrome Data Browser (http://cistrome.org/db/#/), we found a significantly enhanced binding peak between FLI1 and the promoter region of NLRP3 on the mouse genome, demonstrating the regulatory potential of FLI1 on NLRP3 (**Figure 4C**).

We detected a significant rise in NLRP3 expression in the liver of cirrhotic mice, a significant decline in the level of NLRP3 after TGP treat-

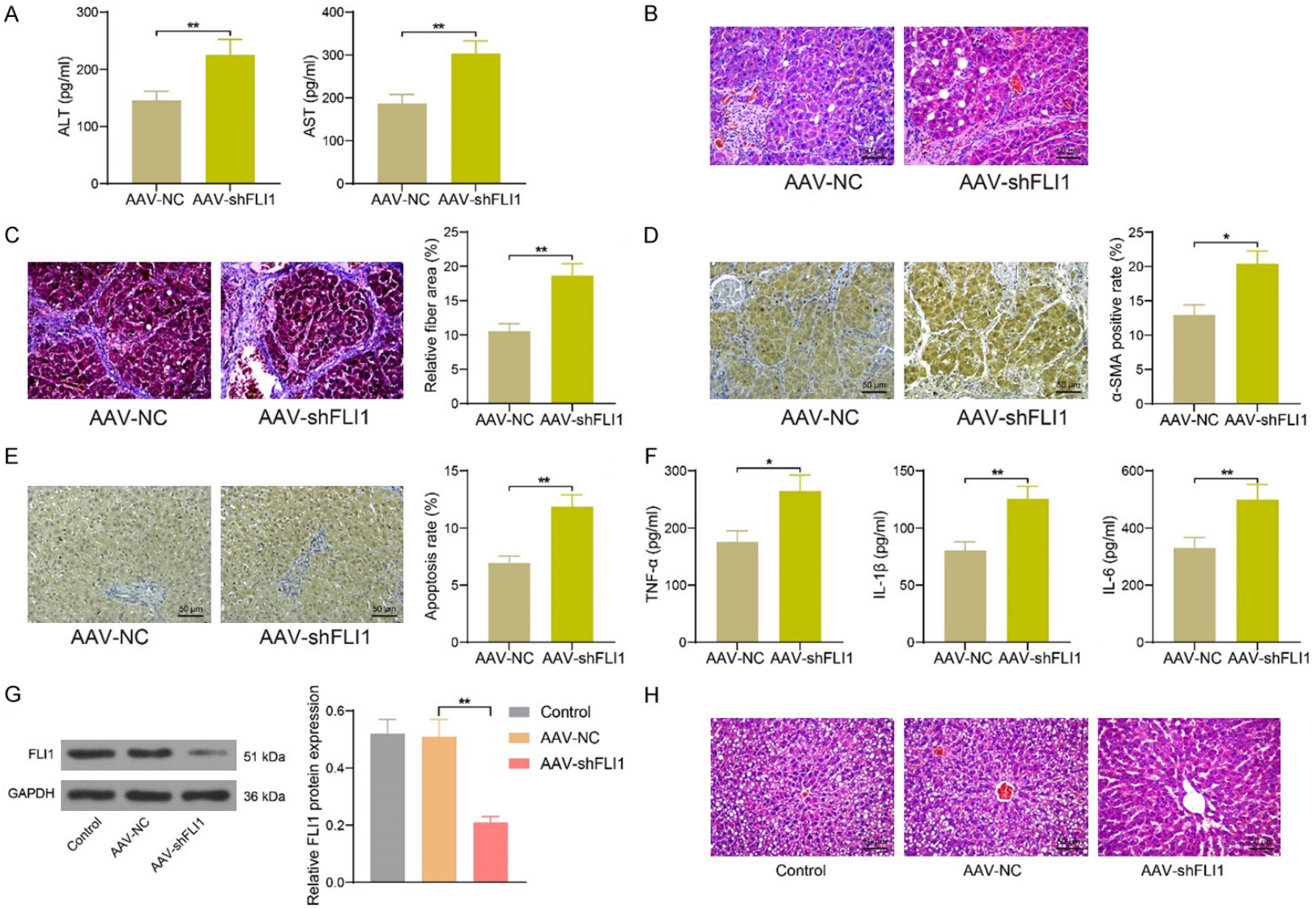
A
ALT (pg/ml)
AST (pg/ml)
AAV-NC
AAV-shFLI1
B
C
Relative fiber area (%)
D
α-SMA positive rate (%)
E
Apoptosis rate (%)
F
TNF-α (pg/ml)
IL-1β (pg/ml)
IL-6 (pg/ml)
G
FLI1
GAPDH
51 kDa
36 kDa
Control
Relative FLI1 protein expression
H

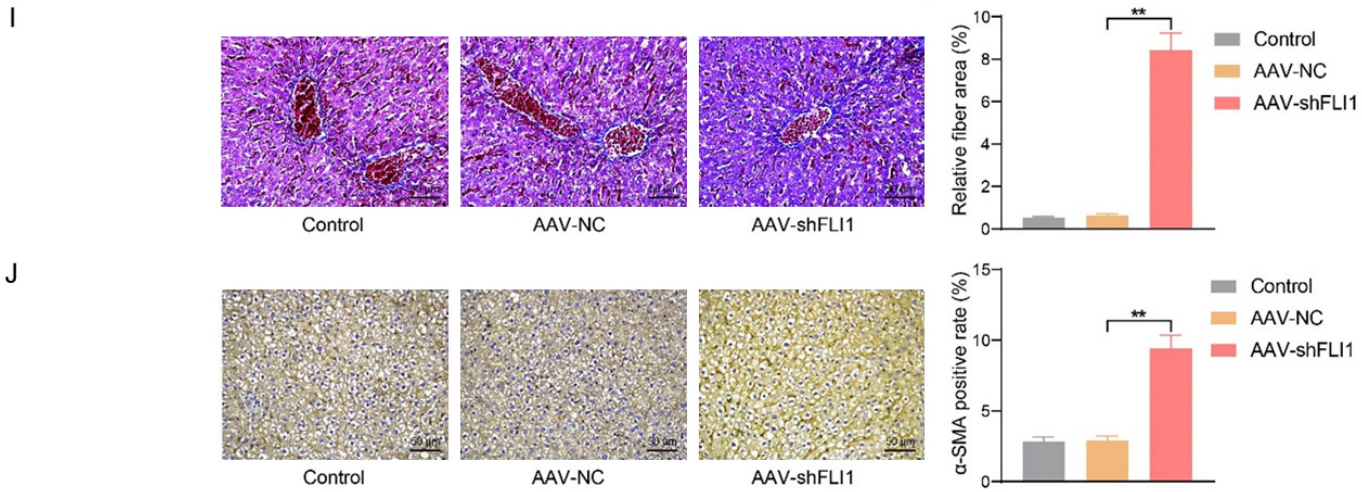

Figure 3. AAV-shFLI1 inhibits the effects of TGP on liver fibrosis and inflammatory responses associated with cirrhosis in mice. Adenoviruses AAV-shFLI1 or AAV-NC were injected into CCl_4 + TGP-treated mice via tail vein injection. A. The serum levels of ALT and AST measured using ELISA in mice. B. The extent of liver tissue damage in CCl_4 + TGP-treated mice assessed using HE staining. C. Fibrosis in the liver of CCl_4 + TGP-treated mice measured using Masson's staining. D. Immunohistochemical analysis of α-SMA positivity in liver tissues of CCl_4 + TGP-treated mice. E. Apoptosis in CCl_4 + TGP-treated mice measured using TUNEL assay. F. The determination of TNF-α, IL-1β and IL-6 in the serum of CCl_4 + TGP-treated mice examined using ELISA assay. Adenoviruses AAV-shFLI1 or AAV-NC were injected into olive oil-treated mice via tail vein injection. G. Detection of FLI1 protein expression in liver tissues of olive oil-treated mice by Western blot (original, full-length gel and blot images can be found in the Supplementary Figure 1). H. The extent of liver tissue damage in olive oil-treated mice assessed using HE staining. I. Fibrosis in the liver of olive oil-treated mice measured using Masson's staining. J. Immunohistochemical analysis of α-SMA positivity in liver tissues of olive oil-treated mice. Data are displayed as the mean ± SD (n = 6) and compared by one-way ANOVA or unpaired *t* test. *P < 0.05, **P < 0.01. FLI1, friend leukemia integration 1 transcription factor; CCl_4, carbon tetrachloride; AAV, adeno-associated virus; NC, negative control; ALT, alanine aminotransferase; AST, aspartate aminotransferase; ELISA, enzyme-linked immunosorbent assay; HE, hematoxylin-eosin; α-SMA, alpha skeletal muscle actin; TUNEL, terminal deoxynucleotidyl transferase (TdT)-mediated 2'-Deoxyuridine 5'-Triphosphate (dUTP) nick end labeling; TNF-α, tumor necrosis factor alpha; IL, interleukin.

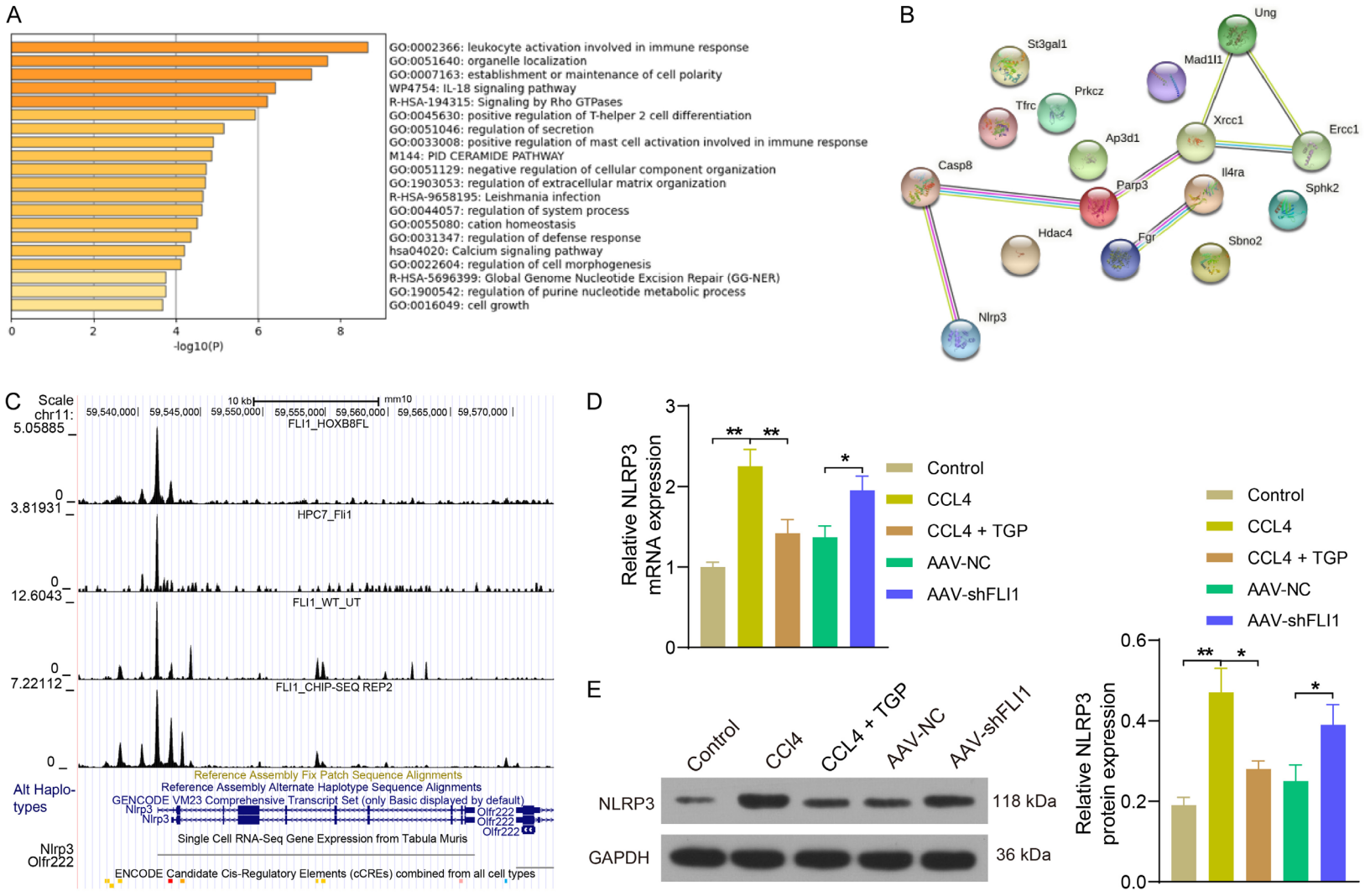
A
GO:0002366: leukocyte activation involved in immune response
GO:0051640: organelle localization
GO:0007163: establishment or maintenance of cell polarity
WP4754: IL-18 signaling pathway
R-HSA-194315: Signaling by Rho GTPases
GO:0045630: positive regulation of T-helper 2 cell differentiation
GO:0051046: regulation of secretion
GO:0033008: positive regulation of mast cell activation involved in immune response
M144: PID CERAMIDE PATHWAY
GO:0051129: negative regulation of cellular component organization
GO:1903053: regulation of extracellular matrix organization
R-HSA-9658195: Leishmania infection
GO:0044057: regulation of system process
GO:0055080: cation homeostasis
GO:0031347: regulation of defense response
hsa04020: Calcium signaling pathway
GO:0022604: regulation of cell morphogenesis
R-HSA-5696399: Global Genome Nucleotide Excision Repair (GG-NER)
GO:1900542: regulation of purine nucleotide metabolic process
GO:0016049: cell growth
0
2
4
6
8
-log10(P)
B
Ung
St3gal1
Mad1l1
Prkcz
Tfrc
Xrcc1
Ercc1
Ap3d1
Casp8
Il4ra
Parp3
Sphk2
Hdac4
Fgr
Sbno2
Nlrp3
C
Scale
chr11:
10 kb
mm10
59,540,000
59,545,000
59,550,000
59,555,000
59,560,000
59,565,000
59,570,000
FLI1_HOXB8FL
5.05885
0
3.81931
HPC7_Fli1
0
12.6043
FLI1_WT_UT
0
7.22112
FLI1_CHIP-SEQ REP2
0
Reference Assembly Fix Patch Sequence Alignments
Alt Haplo-types
Reference Assembly Alternate Haplotype Sequence Alignments
GENCODE VM23 Comprehensive Transcript Set (only Basic displayed by default)
Nlrp3
Olfr222
Single Cell RNA-Seq Gene Expression from Tabula Muris
ENCODE Candidate Cis-Regulatory Elements (cCREs) combined from all cell types
D
Relative NLRP3 mRNA expression
0
1
2
3
**
**
*
Control
CCL4
CCL4 + TGP
AAV-NC
AAV-shFLI1
E
Control
CCl4
CCL4 + TGP
AAV-NC
AAV-shFLI1
NLRP3
118 kDa
GAPDH
36 kDa
Relative NLRP3 protein expression
0.0
0.2
0.4
0.6
**
*
*

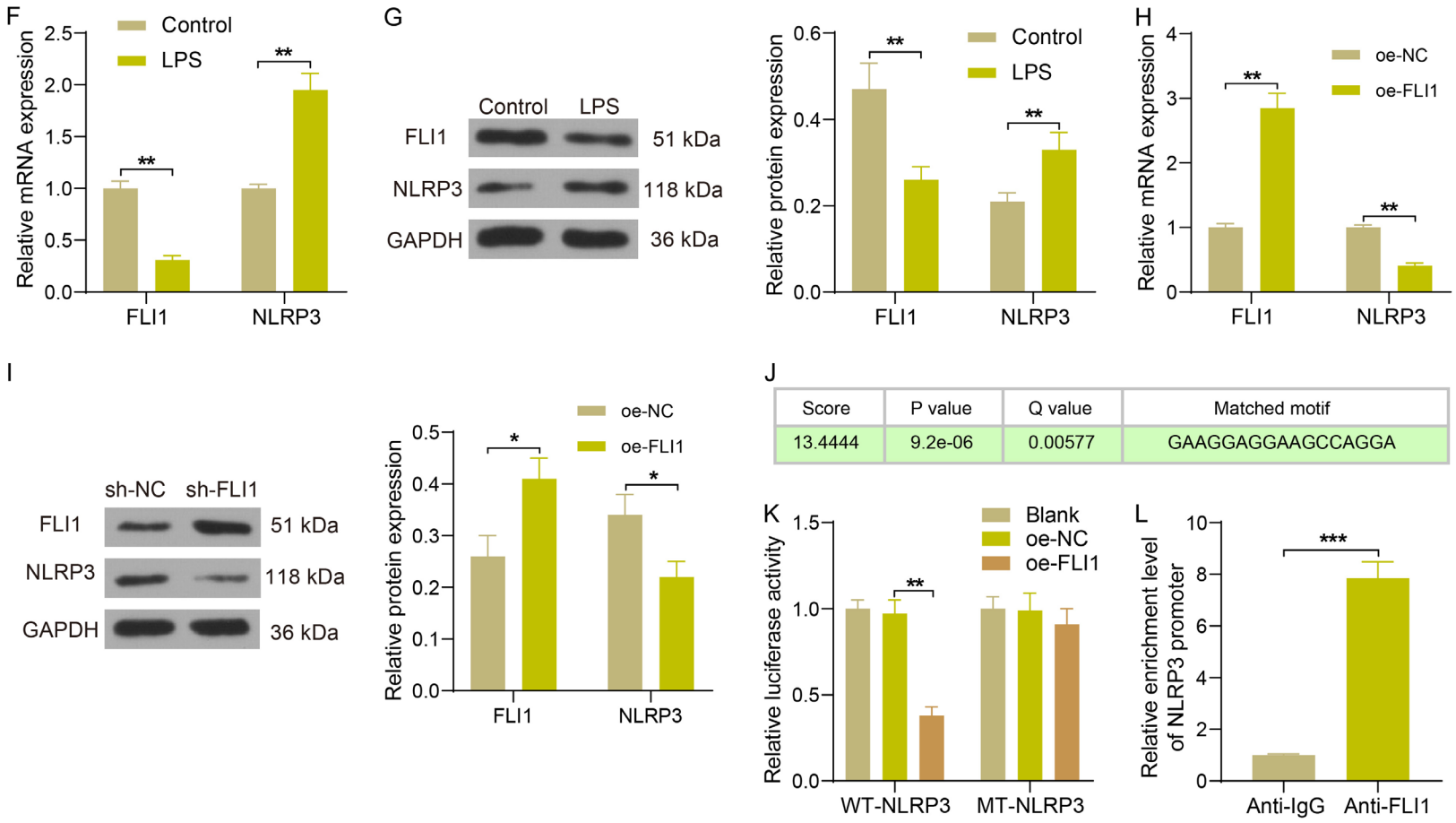

Figure 4. FLI1 represses NLRP3 transcription. (A) Pathway enrichment analysis of downstream targets of FLI1. (B) Protein-protein interactions (PPI) enrichment analysis of downstream targets of FLI1. (C) FLI1 has a possible binding relation with the NLRP3 promoter region. (D, E) Expression of NLRP3 in the liver of mice with cirrhosis by RT-qPCR (D) and Western blot (E) (original, full-length gel and blot images can be found in the Supplementary Figure 1). (F, G) Expression of FLI1 and NLRP3 in LPS-treated mouse hepatocytes assessed by RT-qPCR (F) and Western blot (G) (original, full-length gel and blot images can be found in the Supplementary Figure 1). (H, I) Effects of transfection with oe-FLI1 on FLI1 and NLRP3 expression in LPS-treated hepatocytes by RT-qPCR (H) and Western blot (I) (original, full-length gel and blot images can be found in the Supplementary Figure 1). (J) Binding site of FLI1 on the NLRP3 promoter. (K) The effect of FLI1 on NLRP3 transcription evaluated using the luciferase reporter assay. (L) The binding relation between FLI1 and NLRP3 promoter measured using ChIP-qPCR. Data are displayed as the mean ± SD of three independent experiments (n = 6) and analyzed by unpaired *t* test or one-way/two-way ANOVA. *P < 0.05, **P < 0.01, ***P < 0.001. FLI1, friend leukemia integration 1 transcription factor; NLRP3, nod-like receptor protein 3; LPS, lipopolysaccharide; ChIP, chromatin immunoprecipitation.

ment, and a partial restoration in the level of NLRP3 after inhibition of FLI1 using RT-qPCR and Western blot assays (**Figure 4D**, **4E**). The expression of FLI1 was significantly decreased in NCTC 1469 cells induced by LPS, while the expression of NLRP3 was considerably increased (**Figure 4F**, **4G**). We transfected oe-FLI1 and its control into LPS-induced NCTC 1469 cells. oe-FLI1 not only increased FLI1 expression but also inhibited NLRP3 expression (**Figure 4H**, **4I**). The FLI1 binding site on the NLRP3 promoter was obtained from hTFtarget (**Figure 4J**). Upregulation of FLI1 significantly inhibited the transcriptional activity of WT-NLRP3 promoter sequence. In contrast, the transcriptional activity of the MT-NLRP3 was not significantly affected (**Figure 4K**). ChIP-qPCR experiments directly demonstrated the ability of FLI1 to bind to the NLRP3 promoter (**Figure 4L**). These findings suggest that FLI1 can repress NLRP3 transcription.

Silencing of NLRP3 attenuates the promoting effect of FLI1 inhibition on liver fibrosis and inflammation in mice

To examine the role of NLRP3 on liver fibrosis and inflammation in mice, we injected TGP-treated cirrhotic mice with AAV-NC + AAV-shNLRP3 or AAV-shFLI1 + AAV-shNLRP3. Western blot analysis showed a significant decline in NLRP3 protein expression upon silencing of NLRP3, but no significant change in FLI1 expression (**Figure 5A**). The results of ELISA showed that AAV-shNLRP3 significantly attenuated the inhibitory effect of AAV-shFLI1 on TGP efficacy, whereas inhibition of NLRP3 alone significantly induced the repressive effects of TGP on the levels of ALT and AST (**Figure 5B**). By HE staining, we observed that inhibition of NLRP3 reversed the accentuation in liver damage caused by AAV-shFLI1 and significantly ameliorated the pathological structural changes in the liver of cirrhotic mice (**Figure 5C**). Meanwhile, it was shown by Masson's staining and immunohistochemical assay that knockdown of NLRP3 inhibited liver fibrosis and decreased α-SMA expression in the liver tissues, which were more pronounced in the livers of mice not treated with AAV-shFLI1 (**Figure 5D**, **5E**). TUNEL staining showed that the apoptosis of murine hepatocytes was significantly reduced after AAV-shNLRP3 injection and the hepatocyte-protective effects of TGP was promoted (**Figure 5F**). Finally, ELISA analysis revealed a substantial decrease in serum levels of TNF-α, IL-1β and IL-6 in mice after further inhibition of NLRP3 (**Figure 5G**). In summary, further silencing of NLRP3 in TGP-treated cirrhotic mice with FLI1 inhibition alleviated histopathological changes in the liver, inhibited apoptosis, and attenuated liver fibrosis and inflammatory responses. Moreover, inhibition of NLRP3 alone further promoted the therapeutic effect of TGP on cirrhotic mice.

Discussion

TGP is comprised of paeoniflorin, hydroxyl-paeoniflorin, paeonin, albiflorin and benzoylpaeoniflorin [16]. The anti-inflammatory, anti-oxidative, and anti-hepatic injury properties of TGP have been proven to be without evident toxic or side effects [17]. In this study, the role of TGP in liver fibrosis and inflammatory responses in the treatment of cirrhosis was investigated. Deletion of FLI1 in mice enhanced cell apoptosis, liver fibrosis and inflammatory responses. Furthermore, mechanistic studies found that FLI1 repressed NLRP3 transcription. Thus, TGP might represent a possible candidate for the treatment of cirrhosis.

TGP has been evidenced to ameliorate pristane-induced lupus nephritis [18], restore intestinal barrier function [19] and delay onset of Sjogren's syndrome [20]. In this study, we found that TGP was effective in repressing liver injury markers (ALT and AST) and pro-inflammatory factors (TNF-α, IL-1β and IL-6) in the serum, and in reducing TUNEL-positive cells, collagen area and α-SMA-positivity in the liver tissues. Similarly, TGP has the potential to be a treatment approach for diabetic liver injury by diminishing liver lipid accumulation and inflammatory response [21]. More specifically, the administration of TGP protected the rats from CCl_4-induced acute liver injury and ALT and AST elevation, in addition to hepatocyte apoptosis and inflammation [22]. The anti-inflammatory effects of TGP have also been validated in Sjögren's syndrome [23], gouty arthritis [24], and kidney ischemia/reperfusion injury [25]. TGP increased viability and hampered apoptosis of hypoxia/reoxygenation-treated renal cells [26]. The tubulointerstitial injury was alleviated and α-SMA expression was reduced in diabetic rats administered orally with TGP [27].

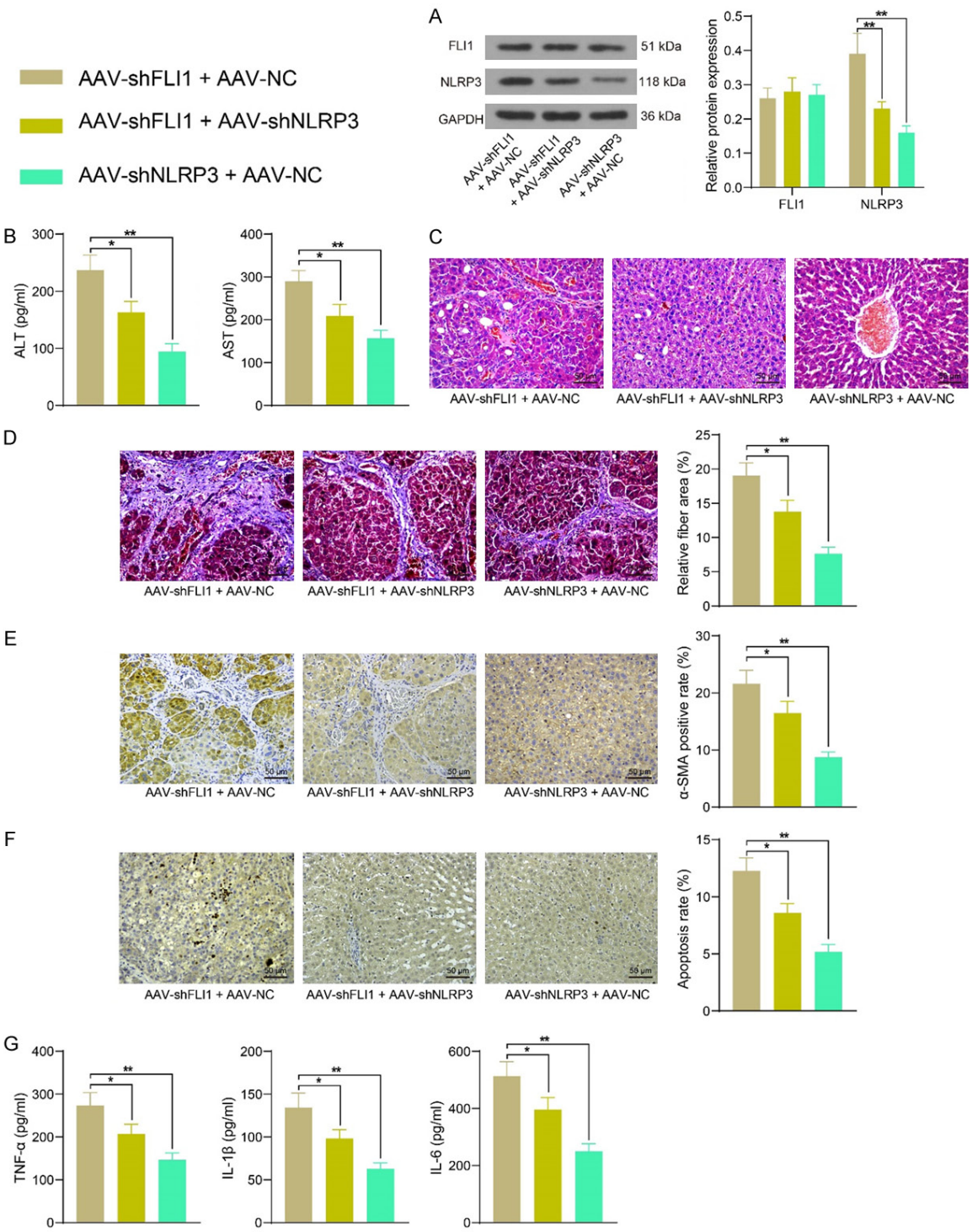

Figure 5. Silencing of NLRP3 mitigates liver fibrosis and inflammatory response in mice treated with AAV-shFLI1 and TGP. TGP-treated mice were injected with AAV-NC + AAV-shFLI1, AAV-NC + AAV-shNLRP3, AAV-shFLI1 + AAV-shNLRP3 via tail vein injection. A. Detection of FLI1 and NLRP3 protein expression in liver tissues of mice (original, full-length gel and blot images can be found in the Supplementary Figure 1) using Western blot. B. The serum levels of ALT and AST were assessed by ELISA in mice. C. The extent of liver tissue damage in mice assessed using HE staining. D. Fibrosis in the liver of mice measured using Masson's staining. E. Immunohistochemical analysis of α-SMA positivity in liver tissues of mice. F. Apoptosis in mice with liver cirrhosis measured using TUNEL assay. G. The determination of TNF-α, IL-1β and IL-6 in the serum of mice examined using ELISA assay. Data are displayed as the mean ± SD (n = 6) and analyzed by one-way/two-way ANOVA. *P < 0.05, **P < 0.01. FLI1, friend leukemia integra-

tion 1 transcription factor; NLRP3, nod-like receptor protein 3; AAV, adeno-associated virus; TGP, total glucosides of paeony; ALT, alanine aminotransferase; AST, aspartate aminotransferase; ELISA, enzyme-linked immunosorbent assay; HE, hematoxylin-eosin; α-SMA, alpha skeletal muscle actin; TUNEL, terminal deoxynucleotidyl transferase (TdT)-mediated 2'-Deoxyuridine 5'-Triphosphate (dUTP) nick end labeling; TNF-α, tumor necrosis factor alpha; IL, interleukin.

Subsequently, we set to decipher the mechanism underlying TGP in cirrhosis. Microarray analysis showed that FLI1 might be the reason for the anti-inflammatory and anti-fibrotic properties of TGP in cirrhosis. Chan *et al.* revealed that FLI1 was a vital mediator of the fibrogenic actions of adenosine in scleroderma [28]. Bujor *et al.* also showed that FLI1 downregulation in scleroderma myeloid cells elicited pro-fibrotic and pro-inflammatory effects [29]. Interestingly, motif analysis of the upstream genomic sequences of hepatocellular carcinoma-associated nonalcoholic fatty liver disease gene module revealed that the enriched motifs were bound by the transcription factor FLI1 [30], indicating the possible interaction of FLI1 and liver diseases. Here, we observed that the loss of FLI1 using AAV-shFLI1 sufficiently repressed the alleviating effects of TGP on liver fibrosis and inflammatory response. In the transcriptome-wide analysis of transcriptional regulators of sensome and inflammation genes in retinal microglia conducted by Saddala *et al.*, FLI1 was revealed as one of the top 10 transcription factors that are differentially expressed between the TNFα/IFNγ-activated and the non-activated microglia [31]. It was thus suggested that the effects of FLI1 on cirrhosis was mediated by its role as a transcription factor.

Integrated bioinformatics prediction showed that NLRP3 is a putative target modulated by FLI1. NLRP3 has been implicated in the pathogenesis of alcohol-associated liver disease, nonalcoholic fatty liver disease/nonalcoholic steatohepatitis, as well as fibrosis [32]. MyD88 in macrophages enhanced liver fibrosis by activating the NLRP3 inflammasome in hepatic stellate cells [33]. As for its individual role, NLRP3 was found increased in renal tubular epitheliums from biopsies of patients with chronic kidney disease, and persistent NLRP3 overexpression was related to chronic pathological changes following acute kidney injury [34]. In addition to its well-known pro-inflammatory effects, exposure to hyperandrogen drives ovarian dysfunction and fibrosis by inducing NLRP3 in mice as well [35]. Knockdown of NLRP3 was revealed here to rescue the effects of AAV-shFLI1 *in vivo*. Also, liver damage induced by bile acid and CCl_4 injection was ameliorated in NLRP3$^{-/-}$ mice, as evidenced by reduced Sirius red-stained areas and a decrease in mRNA expression of α-SMA [36, 37].

Here, we concentrated on the role of TGP in liver fibrosis and inflammatory responses in a mouse model of cirrhosis. Our studies specifically prove that: (1) TGP alleviates cell apoptosis, liver fibrosis and inflammatory responses in mice; (2) TGP exerts its function in cirrhosis by promoting the expression of FLI1; (3) knockout of FLI1 accentuates cirrhosis in mice in the presence of TGP; (4) FLI1 modulates the transcription of NLRP3; (5) knockout of NLRP3 further ameliorates the effects of shFLI1 on mice. There are also limitations in this study, such as the absence of results regarding the phenotype of NCTC 1469 cells in vitro after gene expression alteration, so additional studies are needed.

Disclosure of conflict of interest

None.

Address correspondence to: Xiaoxing Xiang, Yangzhou University Medical College, No. 136, Jiang Yang Middle Road, Yangzhou 225009, Jiangsu, P. R. China. Tel: +86-0514-87978804; Fax: +86-0514-87978804; E-mail: xiaoxing7261@163.com

References

[1] Tsochatzis EA, Bosch J and Burroughs AK. Liver cirrhosis. Lancet 2014; 383: 1749-1761.
[2] Gines P, Krag A, Abraldes JG, Sola E, Fabrellas N and Kamath PS. Liver cirrhosis. Lancet 2021; 398: 1359-1376.
[3] Poordad FF. Presentation and complications associated with cirrhosis of the liver. Curr Med Res Opin 2015; 31: 925-937.
[4] Caligiuri A, Gentilini A, Pastore M, Gitto S and Marra F. Cellular and molecular mechanisms underlying liver fibrosis regression. Cells 2021; 10: 2759.
[5] Roehlen N, Crouchet E and Baumert TF. Liver fibrosis: mechanistic concepts and therapeutic perspectives. Cells 2020; 9: 875.
[6] Jiang H, Li J, Wang L, Wang S, Nie X, Chen Y, Fu Q, Jiang M, Fu C and He Y. Total glucosides of paeony: a review of its phytochemistry, role in

autoimmune diseases, and mechanisms of action. J Ethnopharmacol 2020; 258: 112913.
[7] Huang Y, Wang H, Chen Z, Wang Y, Qin K, Huang Y, Shen P, Ba X, Lin W and Tu S. Synergistic and hepatoprotective effect of total glucosides of paeony on ankylosing spondylitis: a systematic review and meta-analysis. Front Pharmacol 2019; 10: 231.
[8] Jia XY, Chang Y, Sun XJ, Wu HX, Wang C, Xu HM, Zhang L, Zhang LL, Zheng YQ, Song LH and Wei W. Total glucosides of paeony inhibit the proliferation of fibroblast-like synoviocytes through the regulation of G proteins in rats with collagen-induced arthritis. Int Immunopharmacol 2014; 18: 1-6.
[9] Jin L, Li C, Li Y and Wu B. Clinical efficacy and safety of total glucosides of paeony for primary Sjogren's syndrome: a systematic review. Evid Based Complement Alternat Med 2017; 2017: 3242301.
[10] Jiang N, Zheng B, Feng Y, Yin L, Liu Y, Cao L, Zheng N, Wu S, Ding B, Huang X, Wang J and Zhan S. A pharmacokinetics-pharmacodynamics study of single-dose total glucosides of paeony capsule on reducing serum total bile acid in hepatic injury rats. Pharm Biol 2021; 59: 769-777.
[11] Shen M, Men R, Fan X, Wang T, Huang C, Wang H, Ye T, Luo X and Yang L. Total glucosides of paeony decreases apoptosis of hepatocytes and inhibits maturation of dendritic cells in autoimmune hepatitis. Biomed Pharmacother 2020; 124: 109911.
[12] Hu Z, Qin F, Gao S, Zhen Y, Huang D and Dong L. Paeoniflorin exerts protective effect on radiation-induced hepatic fibrosis in rats via TGF-beta1/Smads signaling pathway. Am J Transl Res 2018; 10: 1012-1021.
[13] Lagares D and Hinz B. Animal and human models of tissue repair and fibrosis: an introduction. Methods Mol Biol 2021; 2299: 277-290.
[14] He YS, Yang XK, Hu YQ, Xiang K and Pan HF. Emerging role of Fli1 in autoimmune diseases. Int Immunopharmacol 2021; 90: 107127.
[15] Asano Y, Markiewicz M, Kubo M, Szalai G, Watson DK and Trojanowska M. Transcription factor Fli1 regulates collagen fibrillogenesis in mouse skin. Mol Cell Biol 2009; 29: 425-434.
[16] Zhang L and Wei W. Anti-inflammatory and immunoregulatory effects of paeoniflorin and total glucosides of paeony. Pharmacol Ther 2020; 207: 107452.
[17] Wang H, Wei W, Wang NP, Wu CY, Yan SX, Yue L, Zhang LL and Xu SY. Effects of total glucosides of peony on immunological hepatic fibrosis in rats. World J Gastroenterol 2005; 11: 2124-2129.
[18] Liang CL, Jiang H, Feng W, Liu H, Han L, Chen Y, Zhang Q, Zheng F, Lu CJ and Dai Z. Total glucosides of paeony ameliorate pristane-induced lupus nephritis by inducing PD-1 ligands(+) macrophages via activating IL-4/STAT6/PD-L2 signaling. Front Immunol 2021; 12: 683249.
[19] Cao XY, Ni JH, Wang X, Feng GZ, Li HD, Bao WL, Wang YR, You KY, Weng HB and Shen XY. Total glucosides of Paeony restores intestinal barrier function through inhibiting Lyn/Snail signaling pathway in colitis mice. Phytomedicine 2021; 87: 153590.
[20] Li CL, He J, Li ZG, Zheng LW and Hua H. Effects of total glucosides of paeony for delaying onset of Sjogren's syndrome: an animal study. J Craniomaxillofac Surg 2013; 41: 610-615.
[21] Xia LL, Zhu QJ and Wu YG. Hepatoprotective effect of peony total glucosides and the underlying mechanisms in diabetic rats. Pharm Biol 2017; 55: 2178-2187.
[22] Li H, Cao W, Lu M, Wu C, Wang X and Niu L. Urinary and serum metabolomics analyses uncover that total glucosides of paeony protect liver against acute injury potentially via reprogramming of multiple metabolic pathways. Evid Based Complement Alternat Med 2017; 2017: 9038260.
[23] Liu G, Wang Z, Li X, Liu R, Li B, Huang L, Chen Y, Zhang C, Zhang H, Li Y, Chen Y, Yin H and Fang W. Total glucosides of paeony (TGP) alleviates constipation and intestinal inflammation in mice induced by Sjogren's syndrome. J Ethnopharmacol 2020; 260: 113056.
[24] Meng Q, Meng W, Bian H, Zheng F, Gu H, Zuo R, Miao X, Zhou Z, Wang L, Wen Z, Ma J and Su X. Total glucosides of paeony protects THP-1 macrophages against monosodium urate-induced inflammation via MALAT1/miR-876-5p/NLRP3 signaling cascade in gouty arthritis. Biomed Pharmacother 2021; 138: 111413.
[25] Chang X, Zhang P, Xu XX and Pang B. Total glucosides of paeony inhibited autophagy and improved acute kidney injury induced by ischemia-reperfusion via the lncRNA TUG1/miR-29a/PTEN axis. Drug Des Devel Ther 2021; 15: 2229-2242.
[26] Chen F, Hu Y, Xie Y, Zhao Z, Ma L, Li Z and Tan W. Total glucosides of paeony alleviate cell apoptosis and inflammation by targeting the long noncoding RNA XIST/MicroRNA-124-3p/ITGB1 axis in renal ischemia/reperfusion injury. Mediators Inflamm 2020; 2020: 8869511.
[27] Zhang W, Zhao L, Su SQ, Xu XX and Wu YG. Total glucosides of paeony attenuate renal tubulointerstitial injury in STZ-induced diabetic rats: role of Toll-like receptor 2. J Pharmacol Sci 2014; 125: 59-67.
[28] Chan ES, Liu H, Fernandez P, Luna A, Perez-Aso M, Bujor AM, Trojanowska M and Cronstein BN. Adenosine A(2A) receptors promote collagen production by a Fli1- and CTGF-mediated mechanism. Arthritis Res Ther 2013; 15: R58.

[29] Bujor AM, El Adili F, Parvez A, Marden G and Trojanowska M. Fli1 downregulation in scleroderma myeloid cells has profibrotic and proinflammatory effects. Front Immunol 2020; 11: 800.
[30] Ge J, Bai Y, Tang B, Wei D and Yan M. The gene signature associated with hepatocellular carcinoma in patients with nonalcoholic fatty liver disease. J Oncol 2021; 2021: 6630535.
[31] Saddala MS, Yang X, Tang S and Huang H. Transcriptome-wide analysis reveals core sets of transcriptional regulators of sensome and inflammation genes in retinal microglia. Genomics 2021; 113: 3058-3071.
[32] de Carvalho Ribeiro M and Szabo G. Role of the inflammasome in liver disease. Annu Rev Pathol 2022; 17: 345-365.
[33] Ge S, Yang W, Chen H, Yuan Q, Liu S, Zhao Y and Zhang J. MyD88 in macrophages enhances liver fibrosis by activation of NLRP3 inflammasome in HSCs. Int J Mol Sci 2021; 22: 12413.
[34] Zheng Z, Xu K, Li C, Qi C, Fang Y, Zhu N, Bao J, Zhao Z, Yu Q, Wu H and Liu J. NLRP3 associated with chronic kidney disease progression after ischemia/reperfusion-induced acute kidney injury. Cell Death Discov 2021; 7: 324.
[35] Wang D, Weng Y, Zhang Y, Wang R, Wang T, Zhou J, Shen S, Wang H and Wang Y. Exposure to hyperandrogen drives ovarian dysfunction and fibrosis by activating the NLRP3 inflammasome in mice. Sci Total Environ 2020; 745: 141049.
[36] Holtmann TM, Inzaugarat ME, Knorr J, Geisler L, Schulz M, Bieghs V, Frissen M, Feldstein AE, Tacke F, Trautwein C and Wree A. Bile acids activate NLRP3 inflammasome, promoting murine liver inflammation or fibrosis in a cell type-specific manner. Cells 2021; 10: 2618.
[37] Nie Y, Liu Q, Zhang W, Wan Y, Huang C and Zhu X. Ursolic acid reverses liver fibrosis by inhibiting NOX4/NLRP3 inflammasome pathways and bacterial dysbiosis. Gut Microbes 2021; 13: 1972746.

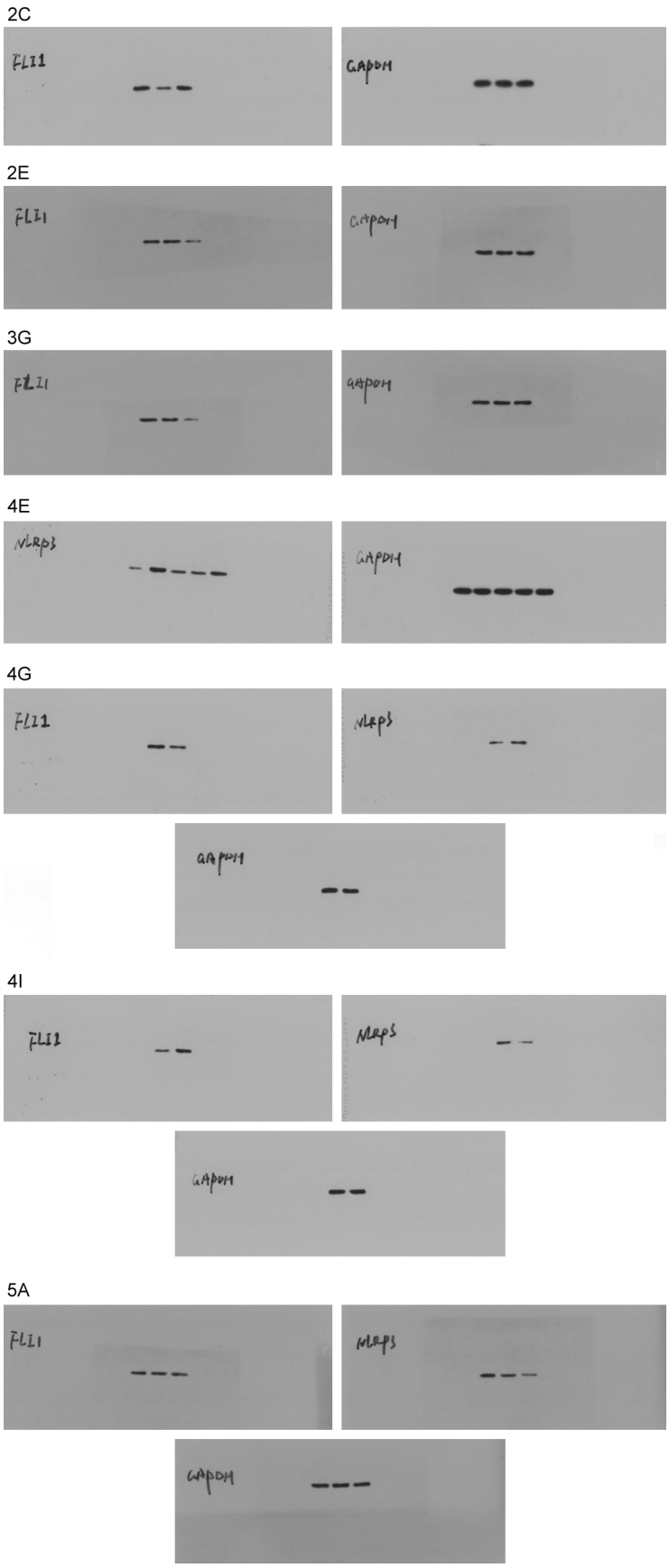

Supplementary Figure 1. Original western blots.